4090 *Chem. Mater.* **2010,** *22,* 4090–4095
DOI:10.1021/cm1009515

CHEMISTRY OF MATERIALS
Article

Giant Magnetic Hardness in the Synthetic Mineral Ferrimagnet $K_2Co^{II}_3(OH)_2(SO_4)_3(H_2O)_2$

Serge Vilminot,*[,†] Peter J. Baker,[‡] Stephen J. Blundell,[‡] Tadashi Sugano,[§] Gilles André,[∥] and Mohamedally Kurmoo*[,⊥]

DCMI, Institut de Physique et Chimie des Materiaux de Strasbourg, UMR 7504 (CNRS-UDS), 23 rue du Loess, BP 43, 67034 Strasbourg Cedex 2, France, Clarendon Laboratory, University of Oxford, Parks Road, OX1 3PU, United Kingdom, Department of Chemistry, Meiji Gakuin University, Yokohama 244-8539, Japan, Laboratoire Léon Brillouin (CEA-CNRS), CEA Saclay, 91191 Gif sur Yvette Cedex, France, and Laboratoire DECOMET, UMR-CNRS 7177, Université de Strasbourg, 4 rue Blaise Pascal, 67070 Strasbourg Cedex, France. † Institut de Physique et Chimie des Materiaux de Strasbourg. ‡ University of Oxford. § Meiji Gakuin University. ∥ Laboratoire Léon Brillouin. ⊥ Université de Strasbourg.

Received April 5, 2010. Revised Manuscript Received May 20, 2010

We present the synthesis, single-crystal X-ray (173 K) and powder neutron (2−30 K) structures and its thermal, optical and magnetic properties of $K_2Co^{II}_3(OH)_2(SO_4)_2(H_2O)_2$. It is a ferrimagnet ($T_C$ = 29.7 K) constructed of $Co_3(OH)_2$ diamond chains connected by sulfate and it displays hysteresis loops ranging from being soft with nearly zero coercivity between 29 and 10 K to very hard reaching coercive field exceeding 70 kOe at 1.8 K. This dramatic change is associated with the changes in domain shape due to the strong exchange anisotropy. Considerable frequency dependence of the ac-susceptibilities is observed in the ordered state. Measurements on a single crystal have established the magnetic axes to be *a*-axis (easy), *b*-axis (intermediate), and *c*-axis (hard).

Introduction

The three most important parameters defining a magnet are the Curie temperature (T_C), remanent field (B, which is related to the magnetization M_{REM}), and coercive field (H_{COER}).[1,2] The last two parameters define the strength or power of a magnet, i.e., the energy product (BH) is related to the amount of energy absorbed upon magnetization.[1−3] To enhance BH, one usually chooses carriers with high moments and fragments the sample to almost the size of single domains to amplify M_{REM}. However, although much is known about what is required to obtain a wide H_{COER}, far less is known about how to control it at the synthetic level. The common element for coercive magnet is a high magneto-crystalline anisotropy energy, which in many cases is obtained by use of carriers with orbital contribution through spin−orbit coupling. Among the first row transition metals, Co^{II}, Fe^{II}, and Mn^{III} are usually the most anisotropic moment carriers. How to control this parameter remains a black art. Not including the intermetallics,[4] such as the Sm−Co and Nd−Fe−B families, several high coercive (hard) magnets have been obtained recently including oxides such as $CoFe_2O_4$[5] and ε-Fe_2O_3,[6] and metal−organic networks such as chains of Mn(TEtOPP)(TCNE)[7] and Mn(TBrPP)$(TCNE)_2$PhMe,[7] where TBrPP = tetra(bromophenyl)porphyrin, TEtOPP = meso-tetrakis(4-ethoxyphenyl)porphyrin, and TCNE = tetracyanoethylene; Co(hfac)2(NN)[8,9] where hfac = hexafluoro-acetylacetonate and NN = 1,3-bis(*N*-tert-butyl-*N*-oxylamino)-5-(1′methyl-1′-(2″-(S)-methylbutoxy)ethylbenzene or *p*-butoxyphenyl-nitronyl nitroxide; layered $AM^{II}M^{III}(ox)_3$[10] where A = bulky organic cation, M^{II} = Mn, Fe, Co, Ni, Cu, and M^{III} = Cr or Fe; pillared-layer $Co_2(OH)_2$(terephthalate);[11] $Co_5(OH)_8$(chdc)·$4H_2O$[12] where chdc = *trans*-1,4-cyclohexanedicarboxylate; interpenetrated layer

*Corresponding author. E-mail: vilminot@ipcms.u-strasbg.fr (S.V.); kurmoo@unistra.fr (M.K.). Tel: 00 33 3 88 10 71 28 (S.V.); 00 33 3 68 85 12 31 (M.K.). Fax: 00 33 3 88 10 72 47 (S.V.); 00 33 3 68 85 15 93 (M.K.).

(1) (a) Herpin, A. *Théorie du Magnétisme*; Presse Universitaires de France, Paris, 1968. (b) Blundell, S. J. *Magnetism in Condensed Matter*; Oxford University Press: Oxford, 2001.
(2) Chikazumi, S. *Physics of Ferromagnetism*; Clarendon Press: Oxford, 1997.
(3) Bertotti, G. *Hysteresis in Magnetism*; Academic Press: London, 1998.
(4) Long, G., Grandjean, F., Eds. *Supermagnets, Hard Magnetic Materials*; NATO Science Series C; Springer: New York, 1991; Vol. *331*.
(5) Hutlova, A.; Niznansky, D.; Rehspringer, J.-L.; Estournes, C.; Kurmoo, M. *Adv. Mater.* **2003**, *15*, 1622.
(6) (a) Jin, J.; Ohkoshi, S.-I.; Hashimoto, K. *Adv. Mater.* **2004**, *16*, 48. (b) Kurmoo, M.; Rehspringer, J.-L.; Hutlova, A.; D'Orleans, C.; Vilminot, S.; Estournes, C.; Niznansky, D. *Chem. Mater.* **2005**, *17*, 1106. (c) Sakarai, S.; Shimoyama, J.-I.; Hashimoto, K.; Ohkoshi, S.-I. *Chem. Phys. Lett.* **2008**, *458*, 333.
(7) (a) Nagai, K.; Iyoda, T.; Fujishima, A.; Hashimoto, K. *Solid State Commun.* **1997**, *102*, 809. (b) Rittenberg, D. K.; Sugiura, K.-I.; Sakata, Y.; Mikami, S.; Epstein, A. J.; Miller, J. S. *Adv. Mater.* **2000**, *12*, 126.
(8) Numata, Y.; Inoue, K.; Buranov, N.; Kurmoo, M.; Kikuchi, K. *J. Am. Chem. Soc.* **2007**, *129*, 9902.
(9) Ishii, N.; Okamura, Y.; Chiba, S.; Nogami, T.; Ishida, T. *J. Am. Chem. Soc.* **2008**, *130*, 24.
(10) Coronado, E.; Galan-Mascaros, J. R.; Gomez-Garcia, C. J.; Martinez-Agudo, J. M. *Adv. Mater.* **1999**, *11*, 558.
(11) (a) Kurmoo, M. *Philos. Trans. R. Soc.* **1999**, *357*, 3041. (b) Kurmoo, M.; Kumagai, H.; Green, M. A.; Lovett, B. W.; Blundell, S. J.; Ardavan, A.; Singleton, J. *J. Solid State Chem.* **2001**, *159*, 343.
(12) Kurmoo, M.; Kumagai, H.; Hugues, S. M.; Kepert, C. J. *Inorg. Chem.* **2003**, *42*, 6709.

 Published on Web 06/09/2010

$(Etrad)_2Co_2\{Cu(opba)\}_3(DMSO)_{1.5}\cdot 0.25H_2O$[13] where Etrad = 2-(1-ethylpyridinium-4-yl)-4,4,5,5,-tetramethylimidazolin-1-oxyl-3-oxide, opba = *o*-phenylene-bis(oxamato); and 3D-rutile $M^{II}(N(CN)_2)_2$[14] where M = Ni or Fe. Here, we report the first example of a synthetic mineral, $K_2Co_3(OH)_2(SO_4)_3(H_2O)_2$, displaying a considerable variation of coercivity from soft (few Oersted) to hard (> 70 kOe for the hard axis) as a function of temperature. We also report the measurements made on a single crystal to define the magnetic anisotropy.

Experimental Section

Sample Preparation. Hydrothermal treatment of an aqueous suspension obtained from $Co(SO_4)\cdot 7H_2O$, K_2SO_4, and KOH in the molar ratio 2:1:1 at 200 °C for 48 h yields $K_2Co_3(OH)_2(SO_4)_3(H_2O)_2$ as violet crystals with elongated plate habit (Figure S2). The sample for neutron diffraction was prepared using D_2O in the place of H_2O. EDX measurements confirm the appropriate ratio of K, Co and S.

General Characterizations. Infrared spectra were recorded using a Digilab Excalibur Series FTIR spectrometer by transmission through KBR pellets containing about 1% of the samples. PXRD were recorded using the Bragg−Brentano geometry on a D8 Bruker diffractometer (Cu Kα = 1.5406 Å) equipped with a front monochromator. EDX analyses for the heavy elements were made using a JEOL 6700 F scanning electron microscope.

Single-Crystal X-ray Structure Determination. Diffraction intensity data were collected on a single crystal mounted on a glass fiber at 173 K using a Bruker CCD diffractometer equipped with Mo Kα radiation. The structure was solved by 3D-Patterson function and refined using SHELXS-97 and SHELXL-97 programs. The details of the best refinement can be found in the CIF file (ESI) that has been deposited at, and can be retrieved from, the Fachinformationzentrum Karlsruhe, 76344-Eggestein-Leopoldshafen, Germany (Crysdata@FIZ-Karlsruhe.de).

Magnetization Measurements. The ac and dc magnetizations were measured for both a polycrystalline sample (45 mg) and one aligned single crystal ($2.0\times 0.8\times 0.3$ mm^3; 1.2 mg; see Figure S2 in the Supporting Information) as a function of temperature (1.8−300 K), field (±70 kOe) and oscillating frequency (17−997 Hz) of the ac field using Quantum Design SQUID magnetometers. Both samples were embedded in polymethylmethacrylate (PMMA) to prevent torque on the crystals in the field. The dc-susceptibility was performed in a field of 100 Oe (powder) or 1 kOe (crystal), and in 3 Oe for ZFC-FC. The ac-susceptibilities were performed in 2 Oe.

Heat-Capacity Measurements. Data were collected on a pressed pellet using a Quantum Design PPMS employing a standard relaxation time technique. Data were corrected for the sample mount and the Apiezon grease used to hold the sample on the mount.

Neutron Diffraction and Magnetic Structure Determination. The neutron diffraction experiments were performed at the Laboratoire Léon Brillouin (CEA Saclay) using the multidetector (800 cells) G4.1 (λ = 2.4226 Å) diffractometer for the determination of the magnetic structure and the thermal evolution study of the low temperature patterns. Seventeen diffraction patterns were recorded in the 2θ range 2°−81.9°, at different temperatures between 1.5 and 40 K. The powder sample was set in a cylindrical vanadium can and held in a liquid helium cryostat. Nuclear and magnetic structures were refined using the FULLPROF program.[27] The nuclear scattering lengths (b_{Co} = 0.2490×10^{-12} cm, $b_K = 0.3670\times 10^{-12}$ cm, $b_S = 0.2847\times 10^{-12}$ cm, $b_O = 0.5803\times 10^{-12}$ cm, $b_D = 0.6671\times 10^{-12}$ cm, $b_H = -0.3739\times 10^{-12}$ cm) and Co^{2+} magnetic form factor were those included in FULLPROF.

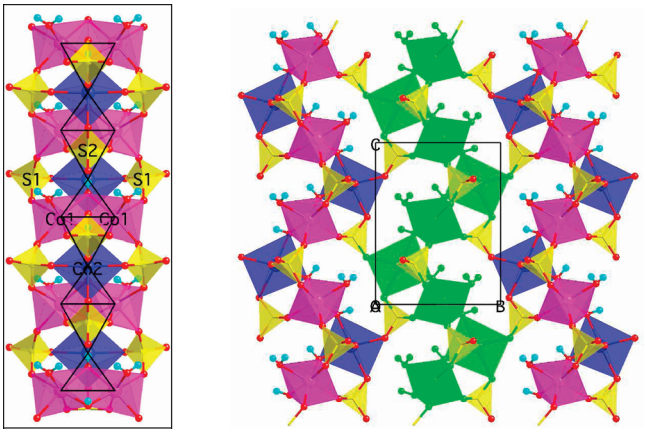

Figure 1. Polyhedral view of a single $Co_3(OH)_2(SO_4)_3$ chain (left) showing the diamond chain magnetic topology (black line) and of the sulfate-bridged connections of the chains into layers (right). The green colored atoms highlight one zigzag chain of cobalt within a layer.

Results and Discussion

X-ray Single-Crystal Structure. The X-ray structure determination on a single-crystal reveals the presence of zigzag chains (Figure 1) of CoO_6 octahedra, one centered at x/a close to 0 and the other close to 1/2, in the *bc*-plane.[15−18] The $Co_3(OH)_2$ chains, parallel to the *a*-axis, consist of two edge-shared Co1 octahedra bridged by Co2 octahedron at the cis-corners through the μ_3−OH (Figure 1). From a magnetic point of view, this topology is described as 'diamond chain'. The sulfate group S1 shares corners with three successive Co1−Co2−Co1 octahedra with the last oxygen atom being terminal. The sulfate tetrahedron around S2 ensures the cohesion between neighboring chains, being corner-shared to one Co2 of one chain and to one Co2 and two Co1 of adjacent chain. Along the chain, the connections of S2 are inversed from one tetrahedron to the next. The polyhedra around the K ions connect the chains yielding a 3D network. The CoO_6 octahedra, 3 oxygen atoms from sulfate, 2 OH and H_2O for Co1, and 4 oxygen atoms from sulfate and 2 OH for Co2, are slightly distorted. The mean Co−O distances are 2.106 and 2.117 Å for Co1 and Co2, respectively. The SO_4 tetrahedra are nearly regular in both cases with a

(13) Vaz, M. G. F.; Pinheiro, L. M. M.; Stumpf, H. O.; Alcantara, A. F. C.; Gohlen, S.; Ouahab, L.; Cador, O.; Mathoniere, C.; Kahn, O. *Chem.—Eur. J.* **1999**, *5*, 1486.
(14) Kurmoo, M.; Kepert, C. J. *New J. Chem.* **1998**, 1525.
(15) Dubler, E.; Oswald, H. R. *J. Appl. Crystallogr.* **1970**, *3*, 175.
(16) Effenberger, H.; Langhof, H. *Monatsh. Chem.* **1984**, *115*, 165.
(17) Zhang, X.-M.; Li, C.-R.; Shang, X.-H.; Zhang, W.-X.; Chen, X.-M. *Chem. Mater.* **2008**, *20*, 2298.
(18) X-ray structure: $Co_3H_6K_2O_{16}S_3$, 613.22 g/mol, 173(2) K, l = 0.71073 Å, orthorhombic, *Cmc*2(1), No. 36, α = 17.8638(12) Å, β = 7.5480(7) Å, χ = 9.7506(7) Å, V = 1314.73(18) Å^3, Z = 4, d = 3.098 Mg/m^3, μ = 4.944 mm^{-1}, $F(000)$ = 1204, Reflections: total = 3283, independent = 1386, R(int) = 0.0331, GOF = 1.019, R1 = 0.0283, wR2 = 0.0559, absolute structure parameter = 0.02(2), Δe (max, min) = 0.620, −0.701 e Å^3.

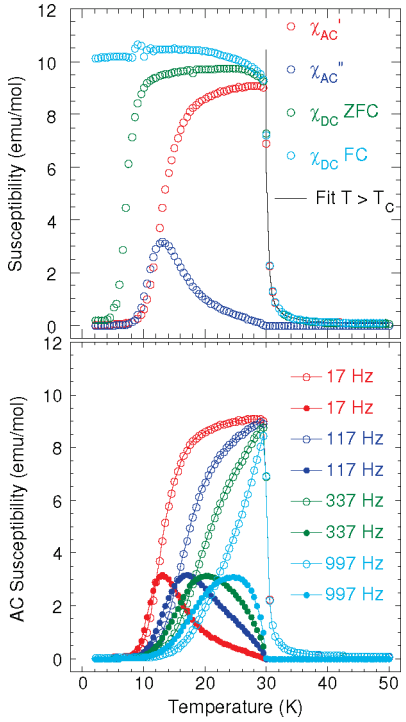

Figure 2. Temperature dependence of the dc and ac magnetic susceptibilities of a polycrystalline sample (top) and the frequency dependence of χ' and χ'' (bottom, χ' and χ'' are represented by open and filled symbols, respectively).

mean S−O distance of 1.474 Å. The coordination number of the K atom is nine with oxygen atoms of three bidentate SO_4, two monodentate SO_4 and one water molecule (a mean K−O distance of 2.956 Å). Although the basic structure within the $Co_3(OH)_2$ chains and the way they are arranged within the layers are the same for the sodium salt, the latter differs in the position and the coordination of the sodium atom and for having two extra water molecules that are coordinated to the sodium atom, attributable to the size of sodium being smaller than that of potassium.[17]

Thermal Properties. Thermogravimetric differential thermal analyses performed in dry air reveal two main weight losses corresponding to the departures of coordinated water and OH groups as H_2O (calcd, 8.8%; obsd, 8.7%) and to the decomposition of part of the SO_4 group as SO_3 (calcd, 26.1%; obsd, 26.7%). The final residue at 1200 °C contains a mixture of K_2SO_4 and CoO.

Magnetic Properties. The ZFC-FC M/H data and those of the ac-susceptibilities as a function of frequency are shown in Figure 2. Spontaneous magnetization, characterized by a bifurcation in the ZFC-FC and nonzero χ'', is observed at 30 K. This long-range magnetic ordering is accompanied by a very sharp lambda-peak in the heat capacity (Figure 3). The estimated magnetic entropy is 16.95 J mol^{-1} K^{-1} after correcting for a lattice background using the sum of a Debye and an Einstein mode, and it corresponds to three $S = 1/2$ cobalt ions. There is an additional anomaly in the magnetization data around 10 K, which is absent in the heat capacity measurement, where the ZFC and FC magnetizations diverge and it is

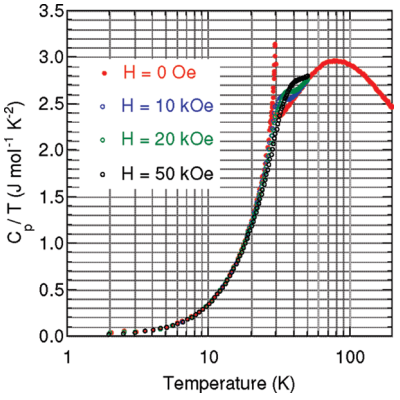

Figure 3. Temperature-normalized molar heat capacity at different applied magnetic fields.

accompanied by a decrease of χ' and a peak of χ''. In the temperature region between the two anomalies, the ZFC and FC dc magnetizations are weakly temperature dependent. In contrast the ac-susceptibilities are very dependent and display a considerable shift with frequency. We note that in the paramagnetic region (50 K > T > 30 K) there is no discernible difference in the magnetization and both the ac and dc data fit well to an exponent $\gamma = 1.18(2)$ with $T_C = 29.7$ K (black line in Figure 2 top). The latter corresponds to the peak in the heat capacity data.

To understand the unusual magnetic behavior described above, we measured the isothermal magnetization at different temperatures (2, 5, 10, 20, and 35 K; see Figure S1 in the Supporting Information) for a polycrystalline sample, where the crystals were fixed in PMMA to prevent torque in the applied field, to cover all the regimes. Measurements at 2 K after ZFC suggest that the 50 kOe field available from the magnet was not enough to saturate the sample, so the data were finally collected following cooling in a field of 50 kOe from 50 K. Because of the saturation problem the hysteresis loop at 2 K was asymmetric with a coercive field of 32 kOe. The asymmetry is not present for the other temperatures and as the temperature of the sample is increased the coercivity disappears quite rapidly. The saturation magnetization measured in 50 kOe tends to increase from those below 10 K to those above. The initial magnetization at 2 K measured following ZFC indicates a multidomain structure exists and a nucleation process is operative.[3] The change of the magnetization with field is consistent with the displacement of domain walls.

For the single crystal (see Figure S2 in the Supporting Information), the magnetizations were studied as a function of field and temperature with the field applied along the three crystallographic axes. ZFC-FC (H = 2 Oe), FC (H = 1 kOe) and isothermal (T = 2 K in field of ±50 kOe and at 1.8 K for field of ±70 kOe) magnetizations indicate that the *a*-, *b*-, and *c*-axes correspond to the easy, intermediate, and hard axis of the magnet, respectively. The ZFC-FC data are similar along the three axes (see Figure S3 in the Supporting Information) and to those for the powder, except for displaying sharper breaks at the Curie temperature. Instead of the noise in the FC data, observed for

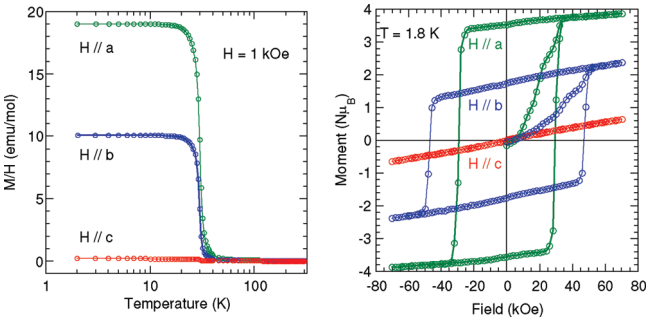

Figure 4. Temperature dependence of dc magnetization in a field of 1 kOe (left) and isothermal magnetizations at 1.8 K (right) along the three orthogonal crystallographic axes of a single crystal.

the powder, for the crystal, an increase is observed at the divergence of ZFC and FC curves. The magnetization in 1 kOe at 300 K is in the order $H // a > H // b \gg H // c$ (Figure 4). They have the following temperature dependences (see Figure S4 in the Supporting Information): the susceptibility data fits the Curie−Weiss equation for $T >$ 150 K with $C = 12.3(1)$, 12.4(1) and 3.7(1) emu K/mol and $\theta = -21(1)$, $-77(2)$ and $-21(3)$ K for $H // a$, $H // b$ and $H // c$, respectively. The average Curie constant per cobalt is 3.2 emu K/mol Co, which corresponds to an effective moment of 5.0 μ_B. The latter is within the range of experimentally observed values.[19] It is worth noting that if we assume the spin quantum number is effectively 3/2 for the high temperatures over which the Curie−Weiss fit were performed, and calculate the g-values along the three axes, we obtained $g_a = 5.12$, $g_b = 5.14$, and $g_c = 2.81$. The nearly equal values for the a- and b-element of the tensor further indicate that the high temperature is well-defined by an XY system.

The isothermal magnetizations at 2 K, following field cooling in 50 kOe from 50 K, display a magnetic hardness that is among the highest recorded.[5−14] The coercive fields are 30 kOe along the easy axis, 47 kOe along the intermediate axis and along the hard axis it is at a field higher than that available (50 kOe) for this SQUID magnetometer. The hysteresis loops are quite square and without any structure. The magnetization in 50 kOe is in the order $M_a > M_b \gg M_c$. The measurements were repeated using another magnetometer equipped with a field of ±70 kOe except that the data were collected after zero-field-cooling and a temperature of 1.8 K (Figure 4). The loops are similar to those after field cooling with similar remanent magnetizations and coercive fields. In addition, we observe virgin magnetization against field clearly demonstrating motion of domain walls along all three axes. We note that the saturation values at 2 K attained on cooling in the field of 1 kOe are slightly inferior to those in a field of 70 kOe. The low saturation value of 1.5 μ_B in 50 kOe for the powder sample being less that that expected (2.3 μ_B) for a ferrimagnet consisting of parallel alignment of the moments of the two Co1 being antiparallel to that of the single Co2 may be due to preferential alignment of the crystals. In contrast, the magnetization averaged of the three orthogonal axes is 2.17 μ_B. Furthermore, if we calculate the g-values along the three axes by considering $M_{sat}(i) = g_i S$ ($i = x$, y, or z) and taking $S = 1/2$ for the low temperatures as indicated by the heat capacity measurements, we get $g_a = 7.6$, $g_b = 4.6$ and $g_c = 0.8$, summing to 13 again. The values suggest a higher anisotropy in the order $a > b \gg c$.

Compared to the results presented above for the potassium salt, the reported magnetic properties for the sodium salt (only available in a powder form) are partly similar. While the temperature dependence of the dc and ac susceptibilities are analogous, the hysteresis loops are quite different. The magnetic properties of this salt were described on the one hand as a single-chain magnet and on the other hand as a ferrimagnet chain with spin-glass-like dynamics.

Neutron Magnetic Structure Determination. A comparison of the neutron powder patterns of a deuterated sample recorded at 1.6 and 40 K, i.e. below and above T_C reveals an increase of the intensity of numerous Bragg reflections, more than 20 and even at high 2θ values. The strongest contributions concern those at 20.13° (110), 24.83° (111), 28.88° (002), 32.93° (202), and 35.43° (112), which coincided with the nuclear Bragg peaks. Such a behavior is characteristic of a ferromagnetic magnetic ordering. However, a weak intensity peak appears at 21.24°, that is not indexed within the nuclear unit cell. Changing the space group to *Pmmm* allows one to index it as (201), which is forbidden in the $Cmc2_1$ space group. A small antiferromagnetic contribution would therefore be expected. Finally, a broad bump in the background is visible with its maximum around 28°. It has been attributed to the presence of a short-range-order magnetic structure. It is visible from 27 K and is still present at the highest measurement temperature.

The associated magnetic structure has been determined with the help of Bertaut's representation analysis method,[24−26] applied to the $Cmc2_1$ nuclear space group with propagation vector k = (0, 0, 0) and Wyckoff positions (8b) for Co1 and (4a) for Co2. Four one-dimensional irreducible representations Γ_1 to Γ_4 are evidenced for both positions. Among them, one describes a purely AF structure, whereas the other ones correspond to ferromagnetic order either along a or b or c axis, respectively. The best fit between observed and calculated profiles is obtained with ferromagnetic order along the a-axis, with a small AF component along b. Moreover, the M_x components for Co1 and Co2 oppose each other, in agreement with the ferrimagnetism suggested by the magnetization measurements. Table S1 in the Supporting Information summarizes the results, and the Rietveld refinement is shown in Figure 5. Figure 6 shows the observed magnetic structure. The magnetic structure is further complicated by the observation of a subtle canting of 12° along the b-axis between pairs of Co1 along each chains. Therefore, we should consider the three sublattices, one consisting of Co2 and the other two of pairs of Co1. The same magnetic structure is observed for all temperatures below T_C. The temperature dependence of

(19) Kurmoo, M. *Chem. Soc. Rev.* **2009**, *38*, 1353.

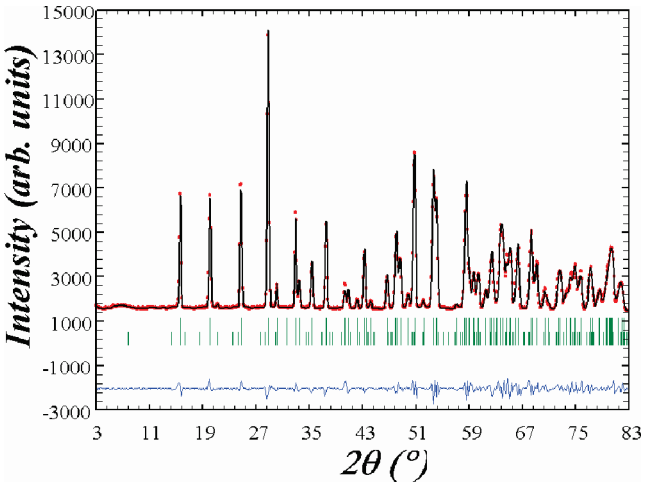

Figure 5. Observed (red symbol) and Rietveld refined (solid black line) data of the neutron diffraction data at 1.6 K. The difference pattern is shown in blue and the upper (nuclear) and lower (magnetic) ticks mark the positions of the Bragg reflections.

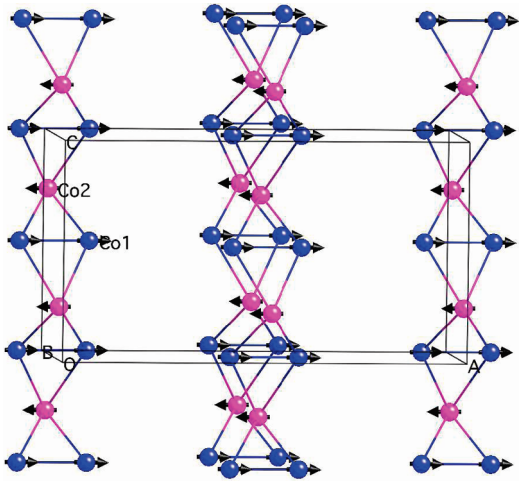

Figure 6. Magnetic structure at 1.6 K: the easy axis is along *a*, the intermediate axis along *b* and the hard axis along *c*. A small canting exists along the *b*-axis for Co1 within each chain. Blue atoms are Co1 and Pink atoms are Co2.

the components of the magnetic moments is shown in figure 7.

Although the magnetic data presented above for the potassium salt appear very complex, there is enough information in them to derive some conclusions. First, the nearly similar values of the susceptibility along a- and *b*-axis can be regarded as those of a *XY*-system and not of a 1D-Ising. Therefore, we can exclude the possibility of single-chain-magnetism. This conclusion is further confirmed by three other observations: (a) the occurrence of long-range ordering (LRO) displayed by the lambda anomaly in the heat capacity data and the presence of strong magnetic Bragg reflections below the critical temperature, (b) the absence of superparamagnetism above the ordering temperature and (c) the sharp cutoff at T_C, and the absolute independence of the ac-susceptibilities on frequency above T_C. It remains now to shed some light on what is happening in the ordered state. First we have established that the principal axes of the magnet to be

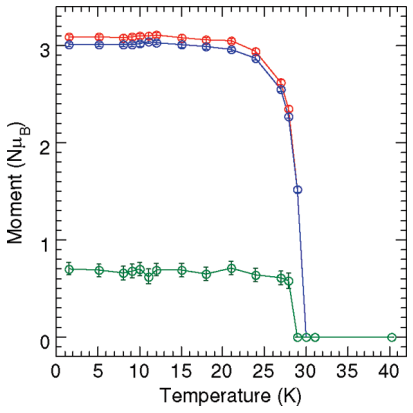

Figure 7. Temperature dependence of the LRO magnetic moments (M_x in blue, M_y in green and M_{total} in red).

a-axis (easy), *b*-axis (intermediate), and *c*-axis (hard). Just below T_C, the hysteresis is that of a soft magnet and this state remains until nearly 10 K. It is to be noted that there is no change in the magnetization along all three axes below T_C but the hysteresis loops start to widen exponentially below 10 K. We believe that this increase may be associated with the domain structure and not with a variation of the single-ion anisotropy. As a soft magnet, the domains are very large and most likely symmetric in shape. When the magnet gets harder, the number of domains increases and their shapes become asymmetric.[3,20] Therefore, in addition to the exchange and shape anisotropy to the barrier for moment reversal, we should add a contribution taking account of the domain shape. We believe the wall motion becomes important as the moments are perpendicular to the chain axis; given that the exchange along the chain axis, via Co−O−Co connection, is expected to be larger than along the other two other axes, via Co−O−S−O−Co connections, the motion of the wall will be anisotropic as well as the anisotropy due to the domain shape. If this model is appropriate, we anticipate an absence of such behavior if the moments are aligned along the chains. This may be the case for the corresponding nickel analogue, where some preliminary measurements show it is also a ferrimagnet with a hysteresis loop having a coercive field of 660 Oe at 2 K. The magnetic properties are quite different to those found for other related cobalt-hydroxy-sulfates.[21−23]

Conclusion

In summary, extensive magnetic measurements on $K_2Co^{II}_3(OH)_2(SO_4)_3(H_2O)_2$, as polycrystalline powder and a single crystal, have demonstrated the largest coercivity of any known mineral magnet. The strong temperature dependence of the coercive field is associated

(20) Craig, D. J.; Tebble, R. S. *Ferromagnetism and Ferromagnetic Domains*; North Holland Publishing: Amsterdam, 1965.
(21) Ben Salah, M.; Vilminot, S.; André, G.; Bourée-Vigneron, F.; Richard-Plouet, M.; Mhiri, T.; Kurmoo, M. *Chem. Mater.* **2005**, *17*, 2612.
(22) Rujiwatra, A.; Kepert, C. J.; Claridge, J. B.; Rosseinsky, M. J.; Kumagai, H.; Kurmoo, M. *J. Am. Chem. Soc.* **2001**, *123*, 10584.
(23) Ben Salah, M.; Vilminot, S.; André, G.; Richard-Plouet, M.; Mhiri, T.; Takagi, S.; Kurmoo, M. *J. Am. Chem. Soc.* **2006**, *128*, 7972.
(24) Bertaut, E. F. *Acta Crystallogr., Sect. A* **1968**, *24*, 217.

with the anisotropic growth of the magnetic domain and is not derived from changes in the single-ion and spin−orbit anisotropy of the moment carrier. Furthermore, the presence of a sharp-lambda peak in the heat capacity rules out the possibility of glassiness and single-chain magnetism previously evoked.

(25) Hovestreydt, E.; Aroyo, I.; Sattler S.; Wondratschek, H. KAREP − a program for calculating irreductible space group representations. J. Appl. Crystallogr., **1992**, *25*, 544.
(26) Rodriguez-Carvajal, J. *BASIREPS−A Program for Calculating Non-Normalized Basis Functions of the Irreductible Representations of the Little Group Gk for Atom Properties in a Crystal*; Laboratoire Léon Brillouin, CEA Saclay: Gif sur Yvette, France, 2004.
(27) Rodriguez-Carvajal, J. *FULLPROF: Rietveld, Profile Matching and Integrated Intensity Refinement of X-ray and/or Neutron Data, 3.5d version*; Léon-Brillouin Laboratory, CEA Saclay: France, 2005.

Acknowledgment. This work was supported by the CNRS (France) and the EPSRC (U.K.). We thank N. Kyritsakas for the collection of the single-crystal diffraction data.

Supporting Information Available: Crystallographic data, IR spectrum, DT-TG analyses, magnetization data, photo of the single crystal used in magnetization measurements, and the Rietveld refinement at 1.6 K (PDF). This material is available free of charge via the Internet at http://pubs.acs.org.